Remote detection of hyperpolarized ^{129}Xe resonances via multiple distant dipolar field interactions with ^{1}H

Le Zhang (张乐),[1,2] Michael Antonacci,[2,3,a)] Alex Burant,[2,3,a)] Karl M. Koshlap,[4] and Rosa Tamara Branca[2,3,b)]

[1]*Department of Applied Physical Sciences, UNC-Chapel Hill, Chapel Hill, North Carolina 27599, USA*
[2]*Biomedical Research Imaging Center, UNC-Chapel Hill, Chapel Hill, North Carolina 27599, USA*
[3]*Department of Physics and Astronomy, UNC-Chapel Hill, Chapel Hill, North Carolina 27599, USA*
[4]*Eshelman School of Pharmacy, UNC-Chapel Hill, Chapel Hill, North Carolina 27599, USA*

(Received 16 June 2016; accepted 4 October 2016; published online 16 November 2016)

A remote detection scheme utilizing the distant dipolar field interaction between two different spin species was proposed by Granwehr *et al.* [J. Magn. Reson. **176**(2), 125 (2005)]. In that sequence ^{1}H spins were detected indirectly via their dipolar field interaction with ^{129}Xe spins, which served as the sensing spins. Here we propose a modification of the proposed detection scheme that takes advantage of the longer T_1 relaxation time of xenon to create a long lasting dipolar field with which the fast relaxing ^{1}H spins are allowed to interact many times during a single acquisition. This new acquisition scheme improves detection sensitivity, but it also presents some challenges. *Published by AIP Publishing.* [http://dx.doi.org/10.1063/1.4964921]

I. INTRODUCTION

^{129}Xe gas has long been considered an ideal NMR sensor. Despite being chemically inert, ^{129}Xe atoms directly and strongly interact with various liquids, solids, proteins, membranes, and different suspensions. As a result, the large and polarizable electron cloud is easily distorted, making its nuclear spin highly sensitive to its immediate chemical environment. This strong sensitivity is reflected in the wide range of ^{129}Xe chemical shifts, which makes this gas an ideal probe for biological systems. Although traditionally a direct observation of the xenon chemical shift is used to probe into the chemical environment in which the gas resides, other approaches such as Spin Polarization Induced Nuclear Overhauser Effect (SPINOE)[1] have also been devised to indirectly probe, via ^{1}H spins, the structures and dynamics of molecules with which xenon comes in direct contact.[2] However, both these approaches require that xenon has some degree of physical contact with the analytes,[3–5] which may limit its usage for the detection of toxic or volatile substances.

To partially overcome this limitation, a remote-sensing scheme was devised by Granwehr and coworkers,[6] where remote detection of ^{1}H spins was achieved by the direct detection of hyperpolarized (HP) ^{129}Xe spins via distant dipolar field (DDF) interactions between the two nuclei. In a highly polarized nuclear spin system, the small dipolar field interaction between nuclear spins residing in different molecules and/or compartments can generate macroscopic signals when pulsed magnetic field gradients are applied to break, in a controlled manner, the symmetry of the nuclear spin magnetization. This interaction has been used in several magnetic resonance spectroscopic and imaging experiments in the past. For example, imaging sequences utilizing DDF have been devised to provide new contrast in magnetic resonance imaging applications,[7,8] to reduce linewidths in magnetic resonance spectroscopy experiments in the presence of large magnetic field inhomogeneities,[9–11] for functional MRI studies,[12,13] for brown adipose tissue detection,[14–16] and to measure temperature *in vivo* with high accuracy.[17,18] The main feature of DDF-based sequences is that the DDF-derived signal comes primarily from pairs of nuclear spins that are separated by a "correlation distance," a user-controllable distance that can be tuned from a few micrometers to several millimeters, allowing sample structures to be probed at a microscopic scale without the loss of sensitivity.[19,20] By changing the correlation distance, this interaction can be tuned to look at spins that are not necessarily in close contact with each other, that are in completely different tissue compartments, or even containers. This was demonstrated by Granwehr and coworkers[6] where the distant dipolar field interaction was used to detect, via HP ^{129}Xe spins, the ^{1}H spins housed in a different sample compartment. The pulse sequence used for this indirect detection scheme is reported in Figure 1(a). In this sequence, the first and second magnetic field gradients are used to spatially modulate the proton and xenon magnetizations such that the dipolar field generated by the modulated longitudinal proton magnetization can partially refocus the transverse xenon magnetization dephased by the second gradient. By selecting a correlation distance smaller than the smallest dimension of the sample, 2D spectra are acquired. These spectra encode the resonance frequency of xenon spins along the directly detected dimension and the resonance frequency of proton spins along the indirectly detected dimension, thus resulting in a remote detection of the proton spectra.

In this work, we propose an alternative detection scheme that switches the roles of proton and xenon spins. Specifically,

a)M. Antonacci and A. Burant contributed equally to this work.
b)Author to whom correspondence should be addressed. Electronic mail: rtbranca@unc.edu

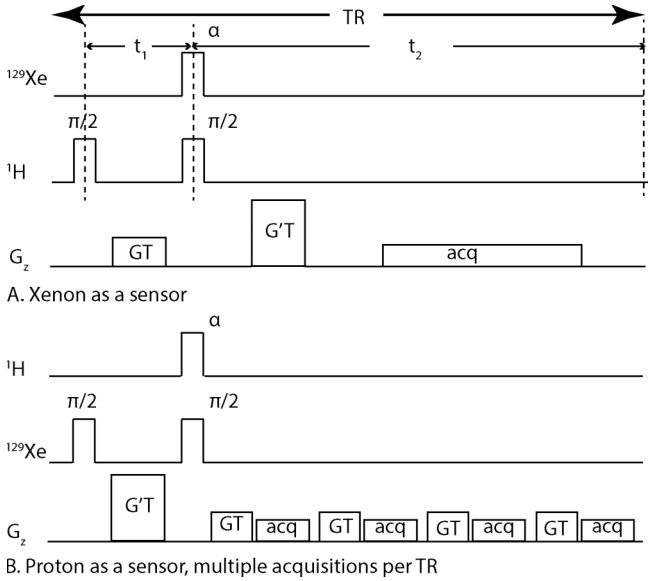

FIG. 1. Indirect detection acquisition scheme. (a) Pulse sequence originally proposed by Granwehr *et al.* (b) Modified scheme in which proton serves as a sensor and the long T_1 of dissolved xenon allows for multiple acquisitions after a single ^{129}Xe excitation and modulation.

we take advantage of the higher gyromagnetic ratio of ^{1}H to improve detection sensitivity and the much longer longitudinal relaxation time of ^{129}Xe dissolved in non-polar solvents, such as methanol and ethanol,[21,22] to produce a long-lasting, modulated longitudinal xenon magnetization with which newly excited and fast-relaxing proton spins are allowed to interact multiple times during a single acquisition. Such an improved acquisition scheme provides an attractive and efficient way to achieve 2D remote detection of xenon frequencies. Experimental, *in vitro* results are presented to demonstrate the feasibility of this approach as well as to explore the potential sensitivity enhancement that the approach could achieve towards the remote detection of heteronuclear NMR spectra.

II. THEORY

The sequence originally proposed by Granwehr *et al.* and the modified sequence proposed in this paper are schematically shown in Figures 1(a) and 1(b), respectively. With respect to the original acquisition scheme, the directly and indirectly detected spin species are swapped and a series of ^{1}H excitation pulses and acquisitions follow after a single modulation of the longitudinal xenon magnetization. In the new sequence, the first 90° excitation pulse is applied only to the xenon channel, while the second excitation pulse is applied to both proton and xenon channels, with a less than 90° flip angle for the former and a 90° flip angle for the latter. The second RF pulse is placed between two pulsed gradients, which are used to modulate the longitudinal and transverse magnetizations, as well as to select a specific coherence pathway and eliminate any spurious proton signal excited by the second RF pulse.

Since a very thorough theoretical derivation of the signal originating from DDF interactions has been presented in a number of publications,[6,23,24] in this paper we provide only a short description of the spin evolution under the new sequence by using the product operator formalism. For simplicity, the effects of diffusion, T_1 and T_2 relaxations, and radiation damping are all ignored. Without the loss of generality, a homogeneous mixture of proton (H) and xenon (S) spins is considered, with ω_H and ω_S being their respective frequency offsets in the rotating frame and in absence of field inhomogeneities. For simplicity, all magnetic field gradient pulses are assumed to be applied along the z direction.

Before the first RF pulse, proton spins (H) are considered to be at thermal equilibrium with a magnetization value of H_0, while xenon spins (S) are typically hyperpolarized with a net magnetization of S_0. The first RF pulse $(\pi/2)_y$ rotates the initial xenon magnetization S_0 into the transverse plane. At the end of the first evolution delay t_1 between the two RF pulses, the S_0 magnetization will have evolved under chemical shift and will be dephased by the first correlation gradient $G'T$ such that it will have the following expression:

$$S_{XY} = S_0 \xrightarrow{\omega_S t_1 S_Z + G'TZ} S_0 \cos(\omega_S t_1 + \gamma_S G'TZ) + \mathrm{i} S_0 \sin(\omega_S t_1 + \gamma_S G'TZ), \quad (1)$$

where γ_S is the gyromagnetic ratio of the xenon nucleus.

The second RF pulse $(\pi/2)_y$ will then rotate the x component of the S magnetization in Eq. (1) to the z axis, while leaving the y component unaffected. As the y component of the magnetization will be subsequently dephased by the second correlation gradient GT, only the z component is retained,

$$S_Z = S_0 \cos(\omega_S t_1 + \gamma_S G'TZ). \quad (2)$$

At the same time, H magnetization will be excited and rotated to the transverse plane, for the first time, by the second RF pulse with a flip angle of α: $H_X = H_0 \sin\alpha$. During the second evolution delay t_2, the transverse magnetization of H spins will evolve under the effect of its chemical shift, while being dephased by the second gradient pulse. During this time, the dipolar field generated by the spatially modulated z-magnetization of S spins, $B_d = \mu_0 \frac{2}{3} S_Z$, will interact with the transverse H magnetization according to the following equation:

$$\frac{\mathrm{d}H_{XY}}{\mathrm{d}t} = \gamma_H H_{XY} \times (B_0 + \mathrm{G'TZ} + \mu_0 \frac{2}{3} S_Z), \quad (3)$$

where γ_H is the gyromagnetic ratio of the proton nucleus and H_{XY} is the transverse magnetization of H spins.

A solution to Eq. (3) can be derived by substituting Eq. (2) into (3) and using a Jacobi-Anger expansion. The condition under which an observable signal can survive is $\gamma_S G' = \gamma_H G$, a condition under which the magnetizations of both S and H spins have the same modulation frequency. When this condition is satisfied, the resulting transverse H magnetization will have the following form:

$$H_{XY} = iH_0 \times \sin\alpha \times e^{\mathrm{i}(\Delta\omega_H t_2 - \Delta\omega_S t_1)} J_1\left(-\frac{2}{3}\gamma_H \mu_0 S_0 t_2\right), \quad (4)$$

where J_1 is the Bessel function of the first kind. Eq. (4) predicts that the evolution of xenon spins is imprinted in the evolution of the proton signal, which can therefore act as an indirect sensor for xenon spins. Since the longitudinal

relaxation time of ^{1}H spins is on the order of few seconds, while the longitudinal relaxation time of xenon is on the order of tens of seconds, multiple ^{1}H excitations and acquisitions can follow a single modulation of the longitudinal xenon magnetization to improve the signal to noise ratio (SNR).

Following the derivation outlined in Granwehr *et al.*, while the original detection scheme is expected to give rise to a maximum xenon signal intensity of

$$|S_{max}| = \frac{\mu_0}{3}\gamma_S^2 B_0 S_0 H_0 T_2^S \sin\alpha \cdot e^{\left(-\frac{t_1}{T_2^H}-1\right)}, \quad (5a)$$

the new detection scheme is expected to give a maximum proton signal intensity of

$$|H_{max}| = \frac{\mu_0}{3}\gamma_H^2 B_0 S_0 H_0 T_2^H \sin\alpha \cdot e^{\left(-\frac{t_1}{T_2^S}-1\right)}, \quad (5b)$$

which gives an increase in sensitivity of

$$\frac{|H_{max}|}{|S_{max}|} \approx \left(\frac{\gamma_H}{\gamma_S}\right)^2 \frac{(\sin\alpha_H)}{(\sin\alpha_{Xe})} \frac{T_2^H}{T_2^S}. \quad (6)$$

Considering the proportionality of the coil noise to $\gamma_H^{1/4}$,[25] the improvement in SNR between the two sequences is expected to be

$$\frac{|SNR_H|}{|SNR_S|} \propto \left(\frac{\gamma_H}{\gamma_S}\right)^{7/4} \frac{(\sin\alpha_H)}{(\sin\alpha_{Xe})} \frac{T_2^H}{T_2^S}. \quad (7)$$

III. METHOD

The sequences were carried out on two different samples, one containing pure ethanol and one containing a mixture of 95%-vol. deuterated methanol with 5%-vol. undeuterated methanol. Samples were prepared as shown in Figure 2.

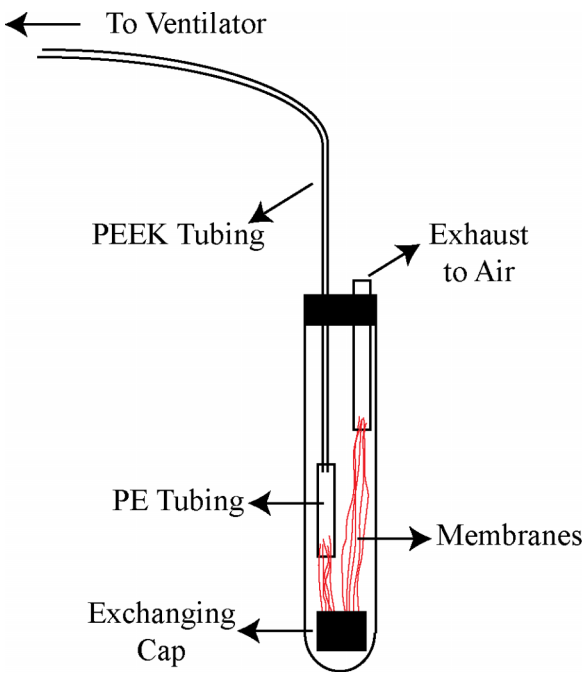

FIG. 2. Experimental setup for gas exchange in the NMR tube.

Samples were placed in a 5 mm medium-walled NMR tube. Two strands of polypropylene micro-porous hollow fiber membranes (Celgard, 150 μm I.D., Membrana, Charlotte, NC) were connected together at the bottom of the NMR tube by capped polyethylene tubings, which allowed efficient exchange of gas between the two strands. The other end of one of the strands was left to open air by polyethylene tubing, while that of the other strand was connected by Polyetheretherketone (PEEK) tubing to the outlet of a home-made ventilator, which pumped polarized xenon into the line once every 30 s.

A direct comparison of SNR between the HP ^{129}Xe spectrum acquired on the methanol and ethanol samples and a thermally polarized ^{129}Xe spectrum acquired on an oil sample with predetermined dissolved-^{129}Xe concentration allowed us to estimate the HP ^{129}Xe concentration in the two samples to be on the order of few mmol/l.

Both sequences were implemented on a Varian Inova 500 MHz NMR spectrometer (McKinley Scientific, Sparta, NJ), where the experiments were conducted using a 1H-19F/15N-31P PFG switchable broadband probe. First and second order shim gradients were used to reduce linewidths. However, because of the presence of the hollow membranes in the active region of the coil, ^{1}H spectral linewidths were bigger than 30 Hz, preventing us from resolving J coupling. All pulses were rectangular pulses with the same flip angle of 90° and a duration of 17 μs. For the pure ethanol sample, both ^{129}Xe and ^{1}H channels were tuned and matched. When ^{129}Xe was used as the sensor (sequence in Fig. 1(a)), we used a flip angle α = 45°, a spectral width of 3000 Hz for both F1 and F2 dimensions, 4096 points in the direct dimension, and 16 increments in the indirect dimension. A TR of 30 s was chosen to allow the transverse magnetization of hyperpolarized ^{129}Xe to fully relax to thermal equilibrium before the next excitation, thus avoiding the excitation of multiple quantum coherences. The spectrum was acquired with a number of averages (NA) of 2 and a single acquisition per TR, for a total acquisition time of 16 min. When proton was used as a sensor (Figure 1(b)), we used the same flip angle α of 45°, a spectral width of 1600 Hz with 16 384 points for the directly detected dimension F2, and a spectral width of 3000 Hz with 16 increments for the indirectly detected dimension F1. The entire spectrum was acquired with TR = 60 s and NA = 2, for a total acquisition time of 32 min. For each TR, each acquisition window was separated by 5 s. A longer TR was chosen to prevent the longitudinal modulated xenon magnetization from being re-excited and further modulated during the second acquisition. In this case, the receiver gain was set to lower values to avoid the saturation of the receiver. In both cases, before Fourier transformation, the indirect dimension was padded to a length of 32 points. For the mixed methanol sample, ^{1}H channel was carefully de-tuned to minimize radiation damping due to extremely high proton magnetization density at high field, while ^{129}Xe channel was tuned and matched. When xenon was used as a sensor (Figure 1(a)), a flip angle of 22° was chosen for the RF pulse on the xenon spin. The t1 dimension was then incremented 24 times at steps of 333 μs, leading to an indirect spectral width of 3000 Hz, equal to the F2 spectral width. The FID (Free Induction Decay) was sampled with a total of 16 384 points for a total acquisition

window time of 1.273 s. The spectrum was acquired with NA = 2 and TR = 30 s, leading to a total acquisition time of 24 min. When proton was used as a sensor (Figure 1(b)), same parameters were used except for the F2 dimension, which was acquired with 16 384 points and a spectral width of 4000 Hz. TR = 60 s and NA = 2 were used, leading to a total acquisition time of 48 min. In both cases, the indirect dimension was zero padded to a length of 48 points before Fourier transformation. To allow replenishing of freshly polarized gas, the acquisition was temporarily suspended after the 8th and 16th increment. To eliminate contamination from protons directly excited by the second 90° pulse, a two-step phase cycling was used in all three sequences. The phases of the second 90° pulse applied to the sensor nucleus as well as the receiver were (x, −x), while the phases of all the other pulses were kept along x. In all cases a correlation distance of 3.5 mm, equal to the diameter of the NMR tube, was selected. This was achieved by setting G equal to 42 mT/m and G′ equal to $G \times \gamma_H/\gamma_{Xe}$ = 151 mT/m, with a duration T equal to 1 ms, when xenon was chosen as the sensor (Figure 1(a)). The two gradients were then swapped when proton was chosen as the sensor (Figure 1(b)). To estimate the sensitivity enhancement produced by the new acquisition scheme, the maximal signal to noise ratio of the 2D spectrum acquired using sequence 1B was directly compared to that of the spectrum acquired using sequence 1A.

To produce hyperpolarized ^{129}Xe, a gas mixture of 1% xenon (26.4% ^{129}Xe content), 10% N_2, and 89% He (Global Specialty Gases, Bethlehem, PA) was made to flow through a Polarean 9800 ^{129}Xe Polarizer (Polarean, Inc., Durham, NC). A mass flow controller was used to regulate the flow rate of the gas mixture to 1.5 Standard Liters per Minute while the hyperpolarized xenon was cryogenically collected for a time of 15 min. The total gas pressure within the optical cell of the polarizer was maintained at 4.2 bars during collection. The temperature of the optical cell was controlled in two ways. First, forced air convection maintained the temperature of the oven, which housed the optical cell at 353 K. Second, heat tape was placed around the pre-saturation bulb of the optical cell and an attached thermocouple kept the temperature of the heat tape at 453 K. Upon completion of the gas collection, HP xenon was dispensed into a 250-ml Tedlar bag (Jensen Inert Products, Coral Springs, FL). The first sample of HP xenon for any study was placed inside a Polarean 2881 Polarization Measurement Station (Polarean, Inc., Durham, NC) to determine the polarization of the sample, with a polarization value of 15% ~ 20% across studies. Subsequent samples were immediately transferred to the ventilator.

The T_1 relaxation times of both proton and xenon spins were measured for the two samples using an inversion recovery sequence on thermally polarized samples prepared by dissolving enriched xenon into the solvent. For the T_1 relaxation measurements of proton spins, the inversion time *TI* was stepped from 0.1 s to 5.1 s with a step of 0.25 s, while the TR was set at 60 s. For the T_1 relaxation measurements of dissolved xenon spins, the *TI* delay was changed from 0.1 s to 90.1 s with a step of 5 s and a TR of 180 s. Additionally, the T_2 times of ethanol protons and ethanol-dissolved xenon were measured using a spin echo sequence, where the delay between the 90° and 180° pulses was stepped from 0.01 ms to 1.26 s with an increment of 20 ms for proton and from 0 to 1.575 s with an increment of 25 ms for xenon. The *TR* was set to be greater than 5 times of the previously measured T_1 of the respective nucleus.

IV. RESULTS

A. T_1 and T_2 measurements

At 11 T, the T_1 time of xenon dissolved in methanol and ethanol was measured to be (18.4 ± 2.5) s and (36.1 ± 3.2) s, respectively. A much shorter longitudinal relaxation was measured, as expected, for methanol protons (4.9 ± 1.3 s) and ethanol protons (3.6 ± 0.8 s). The T_2 time of ethanol protons and of xenon dissolved in ethanol was measured to be (0.581 ± 0.055) s and (1.98 ± 0.08) s, respectively. The T_2 relaxation times of methanol protons and xenon dissolved in methanol were measured to be, using the same method, (0.205 ± 0.016) s and (1.05 ± 0.09) s, respectively.

B. Pure ethanol sample

Figure 3 shows the single pulse ^{129}Xe and ^{1}H spectra. In Figure 3(a) the dominant ^{129}Xe-dissolved-in-ethanol peak can be observed at about 163 ppm away from the gas phase peak at 0 ppm.[26] The relative intensity of the two peaks suggests an efficient exchange of xenon through the hollow fiber membrane. The right figure inset shows the resonance frequency offset at which the dissolved phase was placed, which was about −440 Hz away from the center frequency of 138.265 126 MHz, and the left inset shows the shape of the gas phase peak. A few glitches, at 90 ppm and

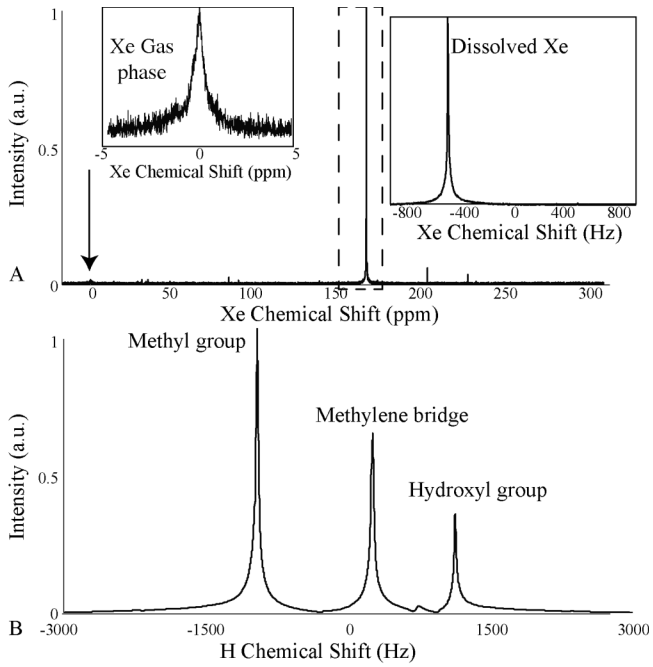

FIG. 3. Proton and xenon spectra acquired on the pure ethanol sample. (a) Xenon spectrum showing both the gas and the dissolved-phase resonance frequencies. (b) Proton spectrum of ethanol.

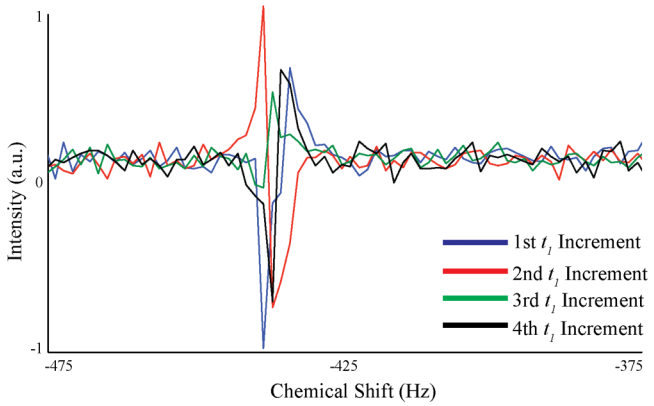

FIG. 4. Phase evolution of the directly detected ethanol-dissolved xenon spectrum under the influence of the dipolar field generated by ethanol protons using sequence 1A.

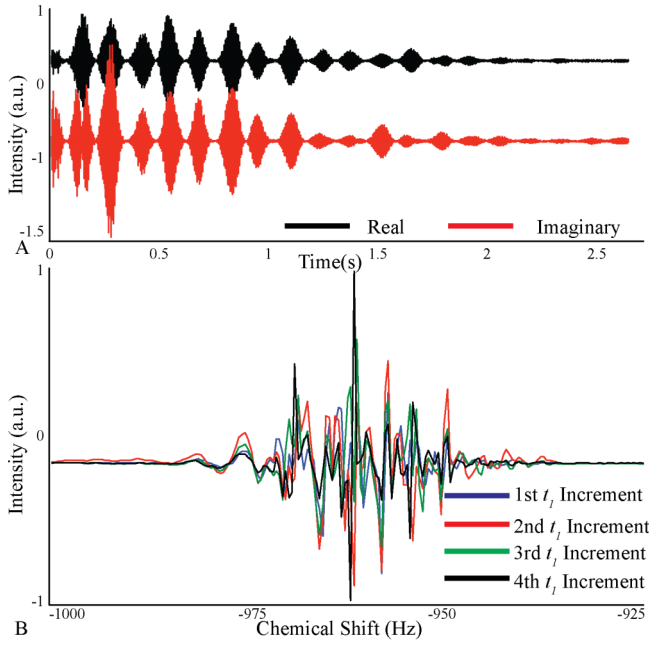

FIG. 5. (a) ^{1}H FID acquired using sequence 1B on the pure ethanol membrane phantom. (b) Phase evolution of the directly detected methyl peak under the influence of the dipolar field generated by methanol-dissolved xenon spins. Radiation damping completely masks the phase evolution.

200 ppm, likely originating from RF interference with outside noise sources, were also observed. Figure 3(b) shows the ^{1}H spectrum of methanol acquired with a center frequency of 499.784 659 MHz, with the methyl group, methylene bridge, and hydroxyl group placed at around −950 Hz, 250 Hz, and 1150 Hz off resonance, respectively. J-coupling of the methyl (triplet) and methylene peak (quartet) was not observed as field inhomogeneities due to the presence of the hollow fiber membranes in the sample led to a FWHM of the methyl peak of about 40 Hz.

Figure 4 shows the phase evolution of the directly detected xenon spectrum (real part only) for the first four indirect time steps. Directly detected proton FIDs and spectra, acquired with sequence 1B that uses proton as the sensor, are shown in Figure 5. Since a multiple acquisition scheme was employed per TR, Figure 5(a) shows the sum of the 4 directly detected FIDs acquired per TR. As pure ethanol has extremely high proton density at high magnetic field, radiation damping can be clearly observed both in the time domain (5A), as well as in the frequency domain (5B), where the phase evolution of the methyl peak during the first 4 t_1 time steps is hard to observe.

Figure 6 shows the 2D spectra acquired using the two sequences. When the xenon is used as a sensor, the intensity of the final signal is linearly proportional to the polarization level of the analyte spins. Since each hyperpolarized xenon gas reservoir was depleted in 16 min, the magnetization of xenon varied significantly between different indirect steps. As a result, a T_1 correction was needed to limit t_1 noise in the indirect dimension. This was achieved by multiplying each

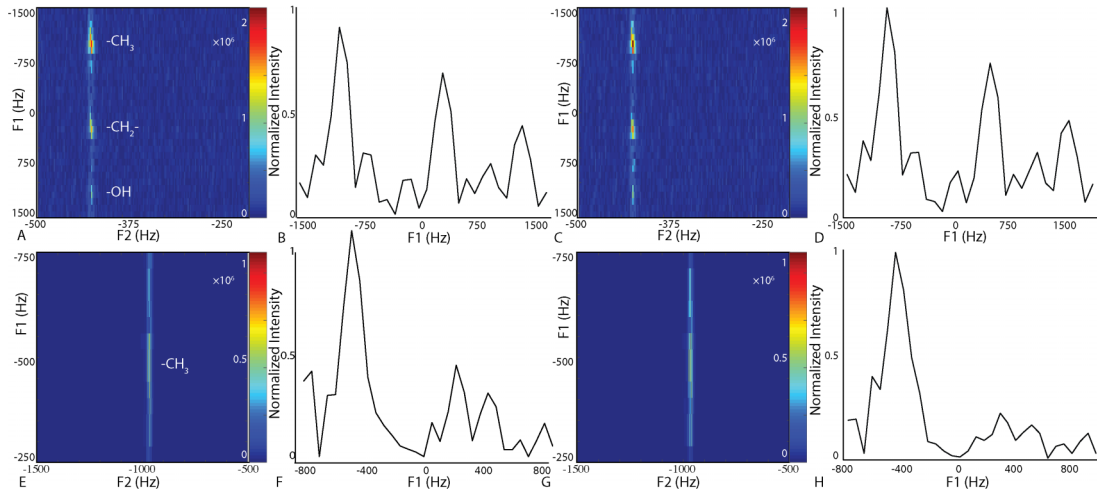

FIG. 6. 2D spectra acquired on the pure ethanol membrane sample. (a) 2D spectrum using sequence 1A without T_1 relaxation correction. (b) F1-projection of the 2D spectrum A, which is normalized to the maximal intensity of spectrum D. (c) 2D spectrum using sequence 1A with T_1 relaxation correction. (d) F1-projection of the 2D spectrum C. (e) 2D spectrum using sequence 1B without T_1 relaxation correction. (f) F1-projection of the 2D spectrum E, which is normalized to the maximal intensity of spectrum H. (g) 2D spectrum using sequence 1B with T_1 relaxation correction. (h) F1-Projection of 2D spectrum G.

nth FID by a factor of $\frac{1}{\exp\{\frac{30\times n}{T1\times 60}\}}$, using a T_1 relaxation time of 38 min for xenon gas outside of the magnetic field.[27] The left, central left, central right, and right columns in Figure 6 show, respectively, 2D spectra without T_1 relaxation correction, indirectly detected spectrum without T_1 relaxation correction, 2D spectra with T_1 relaxation correction, and the indirectly detected spectrum with T_1 relaxation correction. All the figures are normalized to the strongest peak in each figure. When the correction for gas polarization is applied to the sequence that sees xenon as sensor, the t_1 noise is reduced and the intensity of all three ethanol peaks increased by 10%~15%. However, when ^{1}H spins are used as sensor, the correction for gas depolarization cannot be easily applied. As shown in Eq. (4), for the second acquisition scheme in which ^{1}H is the sensor, the magnetization of xenon spins is not simply related to the signal intensity, but it is related to the dipolar demagnetization time $\tau_d = \frac{1}{\gamma_H \mu_0 S_0}$, which directly affects the signal refocusing time, as well as the signal intensity. Figures 6(c) and 6(f) also show, respectively, the indirectly detected ethanol spectrum, with all three main peaks visible, and the indirectly detected xenon spectrum, where the prominent ethanol-dissolved xenon peak dominates.

Figures 5 and 6 clearly indicate that radiation damping in a highly protonated sample is the main issue when ^{1}H is used as a sensor, leading to turbulent spin dynamics.[28] As a result, sequence 1B in this case did not lead to an improvement in the directly detected signal intensity compared to sequence 1A. However, in spite of the presence of radiation damping, which considerably broadened the resonance frequency lines, the indirectly detected ^{129}Xe frequency was still observable. The maximal signal intensity to noise ratio, on the other hand, showed a two-order-of-magnitude enhancement, far exceeding the theoretical value of 2.78. This enhancement, however, is very likely erroneous due to the severe radiation damping.

C. Mixed deuterated/undeuterated methanol sample

Studies on the mixed deuterated/undeuterated methanol sample followed the same protocol described in Sec. IV B. Single pulse spectra of ^{129}Xe and ^{1}H were first acquired to determine the resonance frequency of the dissolved ^{129}Xe as well as undeuterated methyl peaks. As shown in Figure 7(a), the resonance frequency of xenon dissolved in methanol was found about 141 ppm away from the gas phase resonance frequency, in agreement with the literature.[26] The inlet shows the dissolved phase peak at −820 Hz off resonance from the xenon center frequency of 138.262 710 MHz. Figure 7(b) shows the ^{1}H spectrum of methanol with the center frequency at 499.785 345 MHz. The methyl and hydroxyl groups were −350 Hz and 400 Hz off resonance, respectively.

The directly detected ^{129}Xe spectrum after Fourier transform by using sequence 1A is presented in Figure 8, where the evolution of the phase of the dissolved xenon peak for the first four F1 steps is plotted. Similar to Figure 4, the dissolved ^{129}Xe peak in Figure 7 was much higher than the gas phase peak, indicating a good gas exchange through the permeable membrane. However, as the undeuterated methanol merely accounted for 5% of the solution by volume, the ^{129}Xe magnetization refocused by the DDF generated by

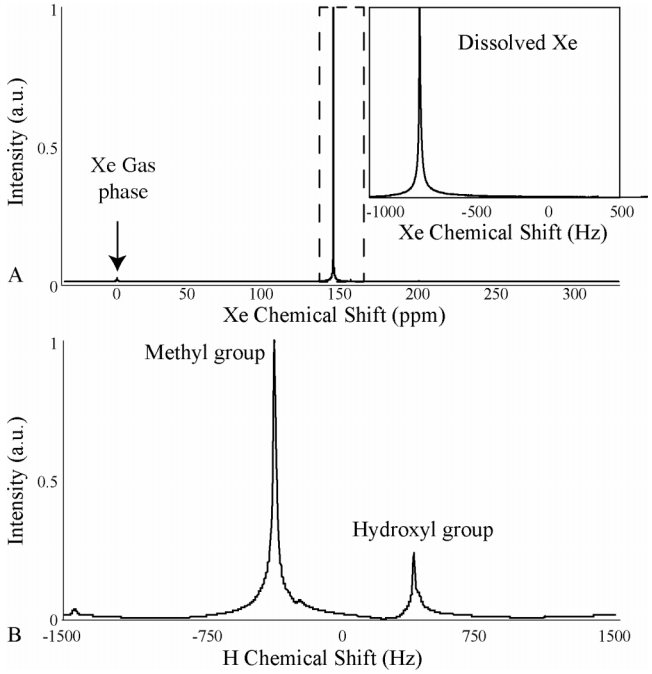

FIG. 7. Proton and xenon spectra acquired on the mixed deuterated/undeuterated methanol sample. (a) Xenon spectrum showing both the gas and dissolved phase peaks. (b) Proton spectrum of methanol.

the undeuterated methanol protons dropped considerably, requiring an increase in the receiver gain.

Figure 9 shows the results obtained using the new acquisition scheme on the methanol sample. As the proton magnetization density is significantly reduced in this deuterated sample, radiation damping is no longer present in the directly detected FID (Figure 9(a)) and the phase evolution of the proton signal from four consecutive indirect steps is clearly present (Figure 9(b)).

The 2D spectra acquired using sequences 1A and 1B and their associated indirectly detected spectra are shown in Figure 10, which are all normalized to the intensity of the strongest peak in Figure 10(c). Figure 10(a) has been corrected for the T_1 relaxation of xenon gas as described above, which again improved the dissolved xenon-methyl group cross peak

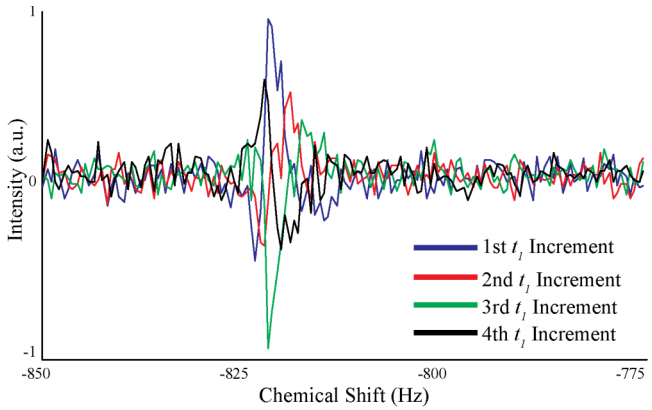

FIG. 8. Phase evolution of the directly detected methanol-dissolved xenon peak under the influence of the dipolar field generated by methanol protons using sequence 1A.

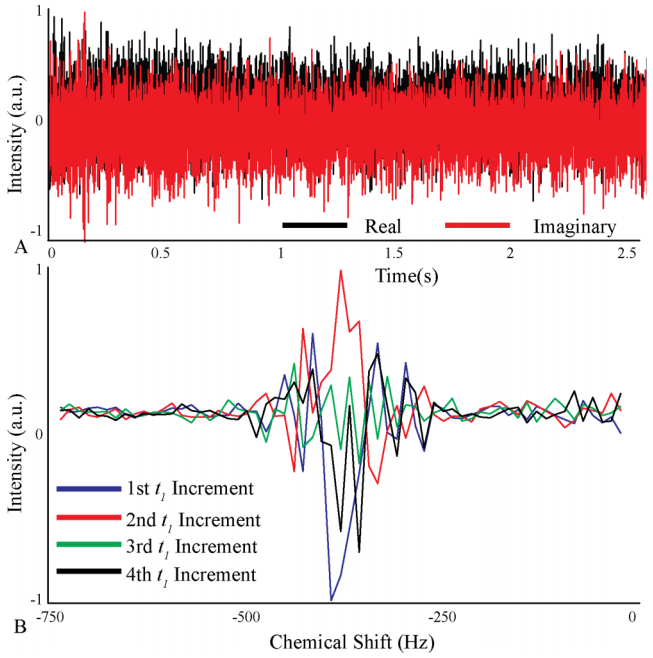

FIG. 9. (a) ^{1}H FID acquired using sequence 1B on the mixed deuterated/undeuterated methanol sample. (b) Phase evolution of the directly detected methyl peak under the influence of the dipolar field generated by dissolved xenon spins. In the absence of radiation damping, the phase evolution is clearly visible.

intensity by 18%. In Figure 10(b), the indirect spectrum of methanol is shown, with both methyl and hydroxyl groups clearly visible. In Figure 10(d), the F1 projection shows the dissolved-phase xenon peak. By comparing Figures 10(b) and 10(d), a clear improvement in the intensity of the signal between dissolved xenon and the methyl group is seen when sequence 1A is replaced by sequence 1B, which amounts to about 18%. Additionally, the indirectly detected dissolved xenon peak also showed a reduced peak width (~200 Hz compared to ~300 Hz in Figure 6(d)). In terms of maximal signal intensity to noise ratio, Figure 10(c) showed a ratio that was 3.2 times as strong as that shown in Figure 10(a), which is consistent with the theoretical prediction of 3.7.

V. DISCUSSION

In this paper, we presented a new acquisition scheme for the indirect detection of ^{129}Xe resonances via the direct detection of ^{1}H resonances. The new acquisition scheme leverages on the much longer longitudinal relaxation time of dissolved ^{129}Xe spins to create a long lasting dipolar field with which the fast relaxing ^{1}H spins are allowed to interact many times. According to Equation (7) and by using the T_2^H and the T_2^s values measured in this study for ethanol and methanol protons and for xenon dissolved in ethanol and methanol, the new acquisition scheme that uses ^{1}H as sensor should lead to an increase in SNR of 2.78 for ethanol and 1.85 for methanol. Moreover, considering that with the new sequence four averages are acquired in a single shot, the theoretical improvement given by the new sequence can be estimated to be 5.56 and 3.7 for ethanol and methanol, respectively.

The new acquisition scheme, when compared to the original one proposed by Granwehr *et al.*,[6] gives an improvement of maximal signal intensity to noise ratio in the 2D spectrum of 3.2, for the methanol sample, only slightly smaller than the predicted enhancement of 3.7. This discrepancy is most likely due to the assumption of the absence of magnetic field inhomogeneities, which would lead to a $\left(\frac{\gamma_H}{\gamma_S}\right)^{7/4}\frac{T_2^{*H}}{T_2^{*S}}$ dependence rather than a $\left(\frac{\gamma_H}{\gamma_S}\right)^{7/4}\frac{T_2^{H}}{T_2^{S}}$ of the signal enhancement. Moreover, the assumption that the modulated longitudinal ^{129}Xe polarization remains identical during the acquisition train and that the maximal signal to

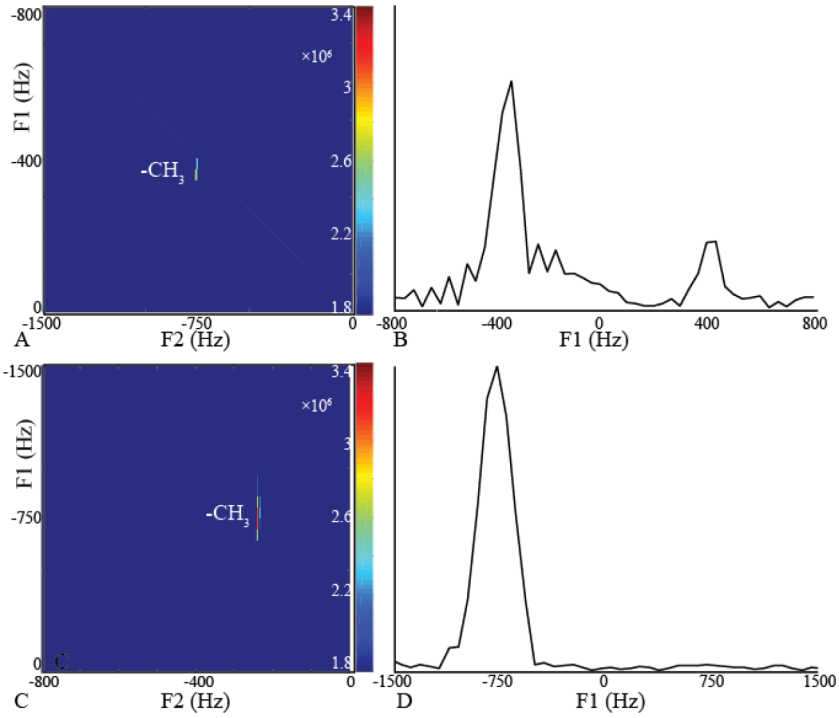

FIG. 10. 2D spectra acquired on the mixed deuterated/undeuterated methanol sample. (a) 2D spectrum using sequence 1A with T_1 relaxation correction. (b) Projection of spectrum A along the indirectly detected dimension F1. (c) 2D spectrum using sequence 1B with T_1 relaxation correction. (d) Projection of spectrum B along the indirectly detected dimension F1.

noise ratio is boosted by a factor of 2 when the result of the 4 acquisition windows is added together may also not be accurate. For the ethanol sample, the apparent enhancement is even bigger, of 100 fold. However, in this case, the presence of radiation damping in the spectrum makes this measurement unreliable.

Despite the increased sensitivity when ^{1}H is used as a sensor, this approach presents several new challenges with respect to the original sequence that uses ^{129}Xe as sensor. The most important issue is the low spin density of dissolved xenon, which we estimated to be on the order of few millimolar or less, creating a substantially weaker dipolar field and, ultimately, leading to a long dipolar demagnetization time during which the proton magnetization rapidly dephases under the effect of magnetic field inhomogeneities, before relaxing back to equilibrium. This means that in solutions where xenon does not dissolve in a relatively high amount to generate a strong magnetization density or in solutions in which the longitudinal relaxation time of xenon is too short, there may not be any sensitivity improvement. Moreover, since the diffusion coefficient of dissolved xenon atoms is larger than that of water molecules, long correlation distances need to be used in order to prevent "scrambling" of the modulation of the ^{129}Xe magnetization by diffusion. This means that this approach is not really feasible when ^{1}H spins are used to sense the xenon gaseous phase. However, it is hard to imagine a situation in which one would want to do that.

It is also worth noting that the improvement in maximal signal to noise ratio in the 2D spectrum provided by the new approach comes with a penalty of a longer acquisition time. Because of the very long T_1 of dissolved ^{129}Xe, sequence B necessitates a very long TR to avoid unwanted excitation of the already modulated longitudinal xenon magnetization. Another issue with this approach may arise from the high magnetization density of ^{1}H at high field, which leads to the observation of radiation damping effects. In these cases, radiation damping will have to be suppressed by using partially deuterated samples as well as by de-tuning the proton channel. Nonetheless this study demonstrates that, although radiation damping can produce considerable noise in the 2D spectrum and broaden the resonance frequency lines, it will not hamper the observation of the indirectly detected species.

VI. CONCLUSIONS

In summary, we have proposed a modification of the previously proposed scheme for remote detection via dipolar field interaction. This method takes advantage of the long spin-lattice relaxation time of dissolved xenon and the high gyromagnetic ratio of protons to generate a long-lasting dipolar field with which ^{1}H spins are allowed to interact many times. The results showed a 3.2 times as strong maximal signal intensity to noise ratio in the 2D spectrum when compared to the sequence proposed for remote detection.

ACKNOWLEDGMENTS

This work was supported by the NIH Grant Nos. DK108231 and DK056350.

[1]A. Kumar, R. R. Ernst, and K. Wüthrich, Biochem. Biophys. Res. Commun. **95**, 1 (1980).
[2]G. Navon, Y.-Q. Song, T. Room, S. Appelt, R. E. Taylor, and A. Pines, Science **271**, 1848 (1996).
[3]M. Schnurr, C. Witte, and L. Schröder, Phys. Chem. Chem. Phys. **15**, 14178 (2013).
[4]T. K. Stevens, R. M. Ramirez, and A. Pines, J. Am. Chem. Soc. **135**, 9576 (2013).
[5]T. Brotin, T. Devic, A. Lesage, L. Emsley, and A. Collet, Chemistry **7**, 1561 (2001).
[6]J. Granwehr, J. T. Urban, A. H. Trabesinger, and A. Pines, J. Magn. Reson. **176**, 125 (2005).
[7]R. Bowtell, S. Gutteridge, and C. Ramanathan, J. Magn. Reson. **150**, 147 (2001).
[8]W. S. Warren, S. Ahn, M. Mescher, M. Garwood, K. Ugurbil, W. Richter, R. R. Rizi, J. Hopkins, and J. S. Leigh, Science **281**, 247 (1998).
[9]D. Z. Balla, G. Melkus, and C. Faber, Magn. Reson. Med. **56**, 745 (2006).
[10]Y. Lin, T. Gu, Z. Chen, S. Kennedy, M. Jacob, and J. Zhong, Magn. Reson. Med. **63**, 303 (2010).
[11]R. T. Branca, E. R. Jenista, and W. S. Warren, J. Magn. Reson. **209**, 347 (2011).
[12]J. T. Schneider and C. Faber, Magn. Reson. Med. **60**, 850 (2008).
[13]W. Richter, M. Richter, W. S. Warren, H. Merkle, P. Andersen, G. Adriany, and K. Ugurbil, Magn. Reson. Imaging **18**, 489 (2000).
[14]R. T. Branca, L. Zhang, W. S. Warren, E. Auerbach, A. Khanna, S. Degan, K. Ugurbil, and R. Maronpot, PLoS One **8**, e74206 (2013).
[15]J. Bao, X. Cui, S. Cai, J. Zhong, C. Cai, and Z. Chen, NMR Biomed. **26**, 1663 (2013).
[16]R. T. Branca and W. S. Warren, Magn. Reson. Med. **65**, 313 (2011).
[17]R. M. Davis and W. S. Warren, Magn. Reson. Med. **74**, 63 (2015).
[18]R. M. Davis, Z. Zhou, H. Chung, and W. S. Warren, Magn. Reson. Med. **75**, 1958 (2016).
[19]L.-S. Bouchard, R. R. Rizi, and W. S. Warren, Magn. Reson. Med. **48**, 973 (2002).
[20]W. Richter, S. Lee, W. Warren, and Q. He, Science **267**, 654 (1995).
[21]S. Mansson, E. Johansson, J. Svensson, L. E. Olsson, F. Stahlberg, J. S. Petersson, and K. Golman, Acta Radiol. **43**, 455 (2002).
[22]N. Segebarth, L. Aïtjeddig, E. Locci, K. Bartik, and M. Luhmer, J. Phys. Chem. A **110**, 10770 (2006).
[23]M. P. Augustine and K. W. Zilm, J. Magn. Reson., Ser. A **123**, 145 (1996).
[24]R. Bowtell, J. Magn. Reson. **100**(1), 1 (1992).
[25]D. Hoult and R. Richards, J. Magn. Reson. **24**, 71 (1976).
[26]K. W. Miller, N. V. Reo, A. J. Schoot Uiterkamp, D. P. Stengle, T. R. Stengle, and K. L. Williamson, Proc. Natl. Acad. Sci. U. S. A. **78**, 4946 (1981).
[27]P. Nikolaou, A. M. Coffey, L. L. Walkup, B. M. Gust, N. Whiting, H. Newton, S. Barcus, I. Muradyan, M. Dabaghyan, G. D. Moroz, M. S. Rosen, S. Patz, M. J. Barlow, E. Y. Chekmenev, and B. M. Goodson, Proc. Natl. Acad. Sci. U. S. A. **110**, 14150 (2013).
[28]S. Y. Huang, Y.-Y. Lin, N. Lisitza, and W. S. Warren, J. Chem. Phys. **116**, 10325 (2002).